MID-AIR PARTICLE MANIPULATIONS BY A 2x2 PMUT ARRAY

Wei Yue¹, Megan Teng¹, Yande Peng¹, Fan Xia¹, Peggy Tsao¹, Yuan Gao¹, Shinsuke Ikeuch², Yasuhiro Aida², Seiji Umezawa² and Liwei Lin¹

¹University of California, Berkeley, USA

²Murata Manufacturing Co., Ltd., Japan

ABSTRACT

This work reports a platform based on ultrasound for mid-air particle manipulations using a 2×2 piezoelectric micromachined ultrasonic transducer (pMUT) array. Three achievements have been demonstrated as compared to the state-of-art: (1) high SPL (sound pressure level) of 120 dB at a distance 12 mm away by an individual lithium-niobate pMUT; (2) a numerically simulated and experimentally demonstrated 2D focal point control scheme by adjusting the phase-delay of individual pMUTs; and (3) the experimental demonstration of moving a 0.7 mg foam plastic particle of 12 mm away in the mid-air by ~1.8 mm. As such, this work shows the potential for practical applications in the broad fields of non-contact actuations, including particle manipulations in microfluidics, touchless haptic sensations, ... etc.

KEYWORDS

Haptic Sensation, LN pMUT, Beamforming, Particle Manipulation.

INTRODUCTION

Mid-air particle manipulation, capable of controlling objects without direct physical contact, is regarded as a crucial tool for applications in property analysis [1, 2], protein crystallization [3], and micro assembly [4, 5]. Ultrasound waves can carry adequate energy and possess relatively short wavelengths, enabling high-resolution mid-air particle manipulations. A common control technique is the Rayleigh's regime scheme [6, 7], which can form acoustic standing waves to cause particles smaller than one-tenth of the wavelength to aggregate at the nodes or antinodes based on their material properties under the influence of acoustic radiation force. Another method involves the beamforming techniques to directly tune the acoustic field around the particles [8, 9] to generate acoustic radiation force for precise manipulation.

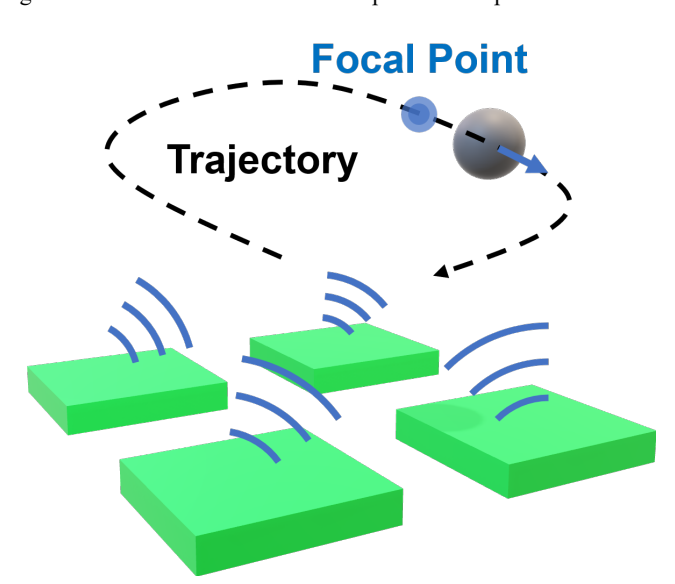


Figure 1: Illustration of the mid-air particle manipulation system by a 2×2 pMUT array. By adjusting the phases of each element, the focal point of the system moves and the induced acoustic radiation force pushes the particle.

Bulk piezoelectric transducers have been widely used in

mid-air particle manipulations, employing strategies that include both the standing wave field [6, 7] and the beamforming scheme [8, 9]. Despite the advantages of piezoelectric micromachined ultrasonic transducers (pMUTs), such as smaller form factor and lower power consumption [10], they have not been utilized for mid-air particle manipulations due to the relatively low-pressure outputs. Recently, high acoustic pressure outputs from pMUTs have been demonstrated with outstanding performance in mid-air haptic feedbacks [11] and mid-air thermal displays [12], offering promising potential for achieving mid-air particle manipulations.

In this work, we report a 2x2 pMUT array by using lithium niobate (LN) as the piezoelectric material. A single pMUT unit shows a high sound pressure level (SPL) of 120 dB at a distance of 12 mm owing to the superior material properties of LN, which leverages the combined effects of high piezoelectric coefficients (i.e., d₃₁ and d₁₁) [13] and the acoustic enhancements from the package design. Furthermore, the pMUT array can achieve inplane focal point control through the beamforming technique to generate steerable acoustic radiation force for basic mid-air particle manipulations.

METHOD

The mid-air particle manipulation system is depicted in Fig. 1, where the green blocks represent pMUT elements, the gray sphere denotes the manipulated particle, and the dashed line illustrates the desired trajectory of the particle within the plane. At each moment, based on the position of the particle, the beamforming technique is employed by adjusting the phase delay of each pMUT element to control the position of the focal point to be precisely behind the particle. This leads to the formation of a strong pressure amplitude gradient around the particle to inducing an acoustic radiation force directed towards the front of the trajectory, thereby propelling the particle along the predesigned path.

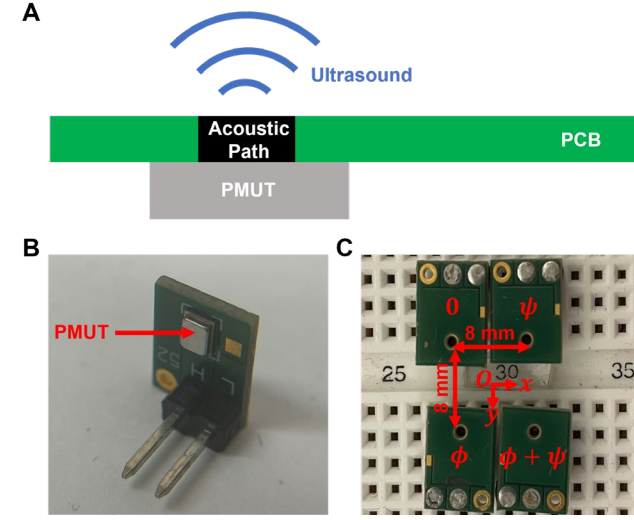


Figure 2: A) The cross-sectional schematic of a single LN-based pMUT with the package. B) The optical image of a single pMUT element with the package. C) The optical image (top view) of the 2×2 pMUT array. The configuration of phase angles follows the rules shown in the diagram, with the position of the focal point within the plane uniquely determined by a pair of ψ and ϕ values.

Fig. 2A presents the cross-sectional schematic of a single packaged LN-based pMUT. The pMUT element is mounted on a PCB measuring 7 mm x 10 mm x 1 mm, positioned directly at the acoustic path. The cross-section of the acoustic path is a circle with a diameter of 1 mm, designed to optimize acoustic pressure for enhanced wave propagation. Fig. 2B illustrates the optical photo of a single LN-based pMUT with the package. On one side of the mounting board, there are two pins connected to the high voltage terminal and low voltage terminal of the pMUT element, respectively. By connecting the positive and negative poles of a power supply or functional generator to these pins, the pMUT can be activated. The 2x2 pMUT array, as shown in Fig. 2C, is assembled with a pitch distance of 8 mm between individual elements (the acoustic holes). The angles marked at each element represent their specific phase angles. The operation principle is the phase delay between different elements rather than the absolute phase angle, the element in the top left corner is marked as 0 degree. Two angles, ψ and ϕ , as indicated in the figure, define the phase delays of elements on the right side with respect to those on the left side, and phase delays of elements on the bottom size with respect to those at the top side, respectively. These angles are used to control the focal point movements in the x- and y-directions, respectively.

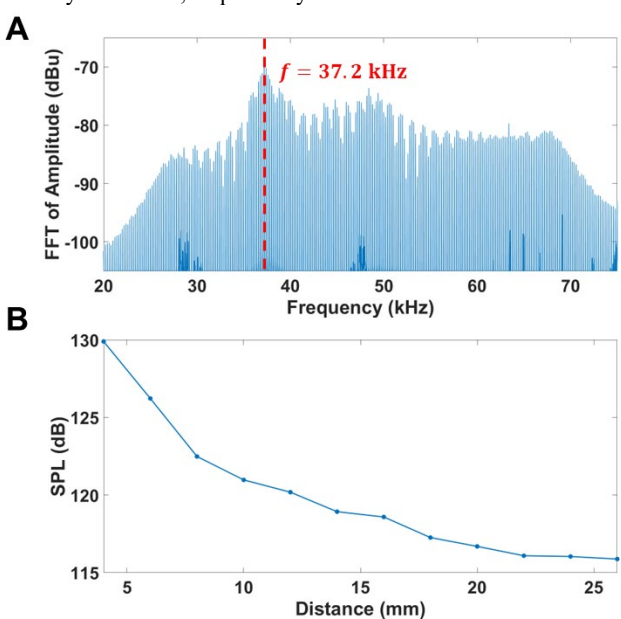


Figure 3: A) The Fast Fourier Transform (FFT) of the measured output pressure from one unit in air. B) Measured sound pressure level (SPL) vs. distance at 37.2 kHz from one unit. A high SPL (sound pressure level) of 120 dB is achieved at a distance 12 mm away in mid-air.

RESULTS AND DISCUSSION Characterization of a Single PMUT

Fig. 3 displays the characterization findings for a single pMUT device. To determine the resonance frequency, a chirp signal of varying frequencies is applied to the pMUT, and the resulting pressure output at a specific point is measured using a microphone (*Bruel & Kjaer 4136*). This chirp signal generated by the arbitrary function generator (*Arbstudio*, *LeCroy*) has the components of equal strength across a range of frequencies (20 kHz ~ 95 kHz). Consequently, the pMUT generates the output sound waves of varying frequencies. The Fast Fourier Transform (FFT) of the pressure amplitude, captured by the microphone, is illustrated in Fig. 3A. The results reveal a resonant frequency at 37.2 kHz. Fig. 3B demonstrates the variations in SPL generated by a single LN-based pMUT with respect to distance at its resonant frequency measured by the microphone. The input is a sinusoidal signal of 0 - 12 V at 37.2 kHz. The specific acoustic

path in the package helps the device to achieve an SPL of 130 dB at a distance of 4 mm and the SPL level is 120 dB at a distance of 12 mm. The low attenuation performance is the result of the using low-frequency ultrasound waves in the air at 37.2 kHz [14]. As such, this work uses a focal point control distance of 12 mm for the prototype tests.

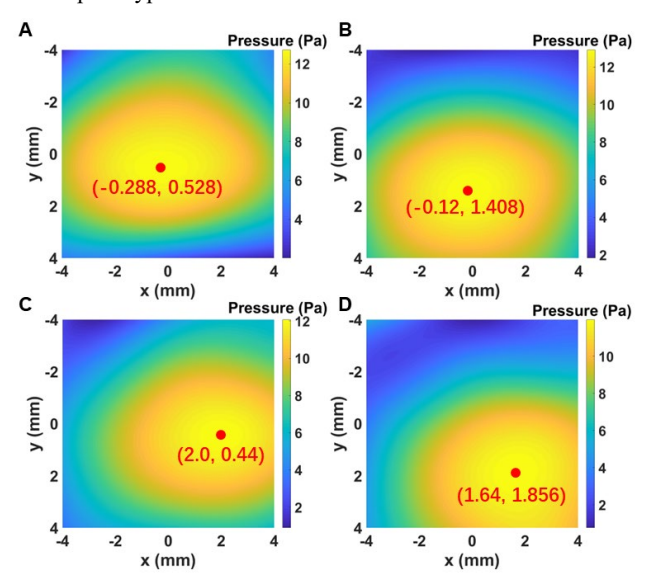


Figure 4: Experimental results of the pressure amplitude field in a plane 12 mm above the array with different phase angles: A) $\phi = 0^{\circ}, \psi = 0^{\circ}, B$ $\phi = 60^{\circ}, \psi = 0^{\circ}, C$ $\phi = 0^{\circ}, \psi = 60^{\circ}$ and **D**) $\phi = 60^{\circ}, \psi = 60^{\circ}$.

In-plane Focal Point Control

The in-plane position of the focal point is defined by the position where the pressure amplitude reaches its maximum, and the beamforming technique is employed to adjust this position. Interference occurs between ultrasonic waves of the same frequency, and the resultant sound field exhibits different properties based on the phase distribution of each ultrasonic beam at the same location. Generally, two waves with a phase difference less than $\pi/2$ will constructively interfere, while those with a phase difference greater than $\pi/2$ will destructively interfere. The calculation of interference also takes into account the direction of each ultrasonic beam depending on their positions. The focal point, which has the maximum pressure amplitude, occurs at the position where multiple sound waves are in phase. If all pMUT elements have the same initial phase, then the focal point will appear at the center of the array, known as the natural focal point. By setting initial phase differences among the pMUT elements, the position of the focal point can be correspondingly altered. For the 2x2 array discussed in this work, the two angles, ψ and ϕ , defined in Fig. 2C, are used to control the position of the focal point within the plane. Fig. 4 presents the measurement results of the pressure amplitude field within the plane at a height of 12 mm, under four representative settings of ψ and ϕ . For each set of ψ and ϕ , the corresponding signal applied to each pMUT element is customized through a four-channel arbitrary function generator (Arbstudio, LeCroy). Each pMUT element receives a sinusoidal signal ranging from 0 to 12 V, with the frequency fixed at 37.2 kHz. The initial phase angle for each channel is determined based on the values of ψ and ϕ . A commercial microphone (Bruel & Kjaer 4136) is placed on a movable platform to sample an area of 8 mm x 8 mm, for the pressure amplitude measurement at discrete points. The overall pressure map throughout the entire region is obtained by interpolating pressure results measured at discrete points. When $\psi = 0^{\circ}$ and $\phi = 0^{\circ}$, no beamforming is performed for a natural focal point near the center of the array, as shown in Fig. 4A. The output performance of each pMUT element is not identical due to

variations in the manufacturing process and experimental parameters. As such, the focal point exhibits a 0.6 mm offset from the center and the pressure amplitude pattern has the elliptical shape instead of a circular shape. Fig. 4B displays the pressure amplitude field with $\psi = 0^{\circ}$ and $\phi = 60^{\circ}$. It is found that as ϕ increases, the focal point moves downward as expected since the ultrasonic waves emitted by the two elements at the top side must travel a greater distance to compensate the phase difference. A phase difference of 60 degrees results in the focal point to shift approximately 0.9 mm. Similarly, as ψ increases, the focal point moves rightward as expected. The pressure amplitude field generated by the array with $\psi = 60^{\circ}$ and $\phi = 0^{\circ}$ is shown in Fig. **4C**. These results show that the variation of ϕ can produce 2 mm more movements for the focal point when compared to those due to the same variation of ψ , probably due to the nonuniformity of the array. Finally, Fig. 4D presents the pressure amplitude field produced with $\psi = 60^{\circ}$ and $\phi = 60^{\circ}$, illustrating the combined effects of changing both ψ and ϕ , for a simultaneous focal point movement to the right and bottom.

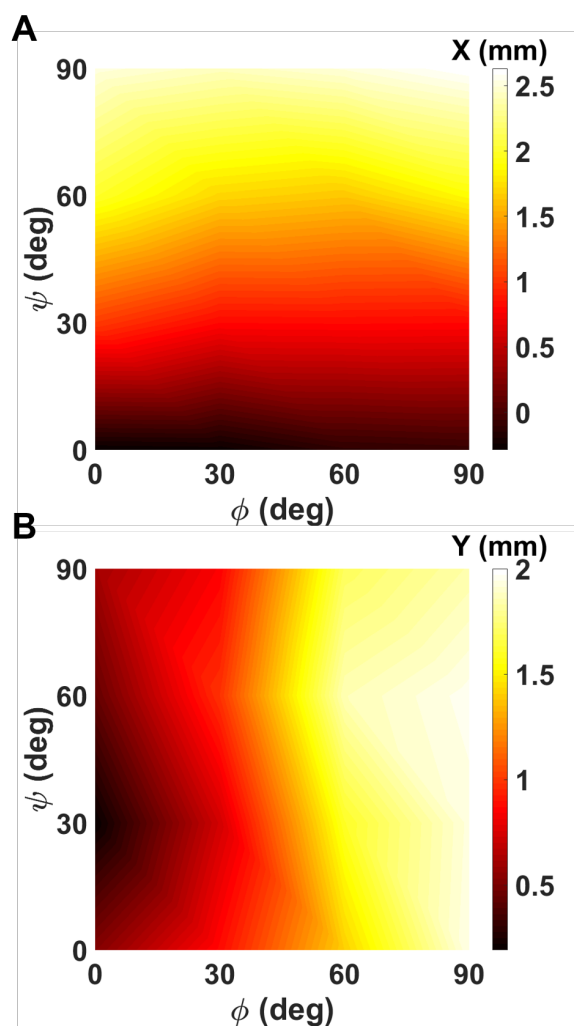


Figure 5: The experimental results showing the focal point positions with respect to different phase angle settings (ϕ and ψ): A) The x-position of the focal point, and B) The y-position of the focal point.

To precisely control the movement of the focal point within the plane, a complete mapping relationship between the focal point position and phase angles, ψ and ϕ , is required. Therefore, the pressure amplitude fields for the entire range of ψ from 0 to 90 degrees and ϕ from 0 to 90 degrees are measured to capture the position of the focal point. For both ψ and ϕ , with a step of 15 degrees, a total of 49 different pressure amplitude fields are

measured. For areas between discrete points, interpolation is used to obtain estimated values. The results are presented in Figs. 5A and 5B for the relationship between the x and y coordinates of the focal point (as defined in Fig. 2C) with respect to the two phase angles, respectively. These results indicate that the x-coordinate of the focal point increases as ψ increases with little correlation with ϕ as expected. Within this given range, the relationship between x and ψ is approximately linear, with an increase of about 0.029 mm per degree for a maximum of 2.6 mm when ψ is 90 degrees. Similarly, in Fig. 5B, the y-coordinate of the focal point increases approximately linearly with ϕ , with an increase of about 0.022 mm per degree for a maximum of 2 mm at 90 degrees and with little correlation to ψ . Due to symmetry, if ψ or ϕ are negative, the corresponding coordinates of the focal point will also be negative, thus mapping the focal point position across the entire range from -90 to 90 degrees for both ψ and ϕ . Generally, the focal point can be adjusted arbitrarily within a 5 mm x 4 mm rectangular area. The results in Fig. 5 will serve as a guide for controlling the position of the focal point in subsequent particle manipulation test to determine the values of ψ and ϕ based on the desired position.

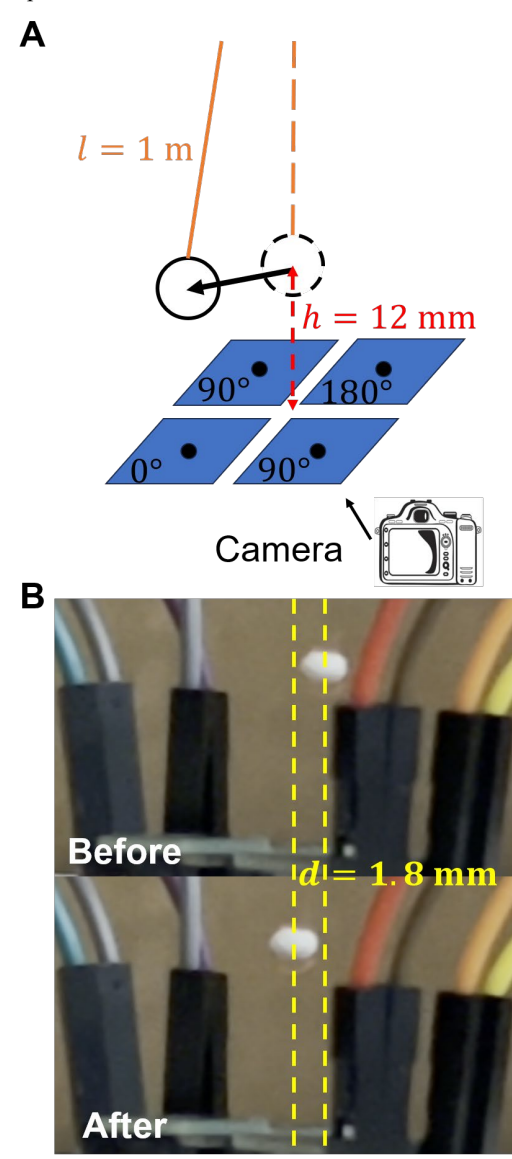


Figure 6: A) The schematic of the particle manipulation experimental setup. B) Side view optical photos of the foam particle before $(\phi = 0^{\circ}, \psi = 0^{\circ})$ and after $(\phi = 90^{\circ}, \psi = 90^{\circ})$ the change in the phase angle settings of the pMUT array. A lateral displacement of ~1.8 mm is observed.

Particle Manipulation

A lightweight foam particle with a mass of 0.7 mg and a radius of 1.8 mm is suspended 12 mm above a 2x2 pMUT array using a fine wire 1 m in length for the particle manipulation test, with the experimental setup shown in Fig. 6A. The gravitational pull on the foam particle is counteracted by the tension provided by the long wire, while the acoustic radiation force generated by in-plane focal point control can push the foam particle to move within the horizontal plane. In practice, by generating a focal point opposite to the desired direction of movement for the particle can move the particle towards the specified direction until it reaches a new equilibrium state. Taking the phase angles labeled in Fig. 6A as an example, with $\psi = 90^{\circ}$ and $\phi = 90^{\circ}$, the focal point shifts towards the topright corner, thereby pushing the foam particle towards the bottom-left corner. This process is captured by a camera positioned perpendicular to the motion of the foam particle, with the results displayed in Fig. 6B. Before changing the phase angle settings ($\psi = 0^{\circ}$ and $\phi = 0^{\circ}$) and after ($\psi = 90^{\circ}$ and $\phi = 90^{\circ}$), the foam particle moved approximately 1.8 mm towards the left side of the frame. This process is repeated five times consecutively to eliminate the randomness caused by other factors, with the foam particle moving to a nearly identical position each time. Based on the mechanical equilibrium equation, the magnitude of the acoustic radiation force acting on the foam particle is calculated to be approximately 0.01 µN. By altering the settings of ψ and ϕ , the foam particle can be propelled to different positions, and a time-varying ψ and ϕ setting allows for continuous particle manipulation.

CONCLUSION

This paper presents a 2x2 LN-based pMUT array designed for mid-air particle manipulation. Leveraging the superior piezoelectric material constant of LN over that of Aluminum Nitride for better acoustic emissions and a welldesigned acoustic package, a single device can generate an SPL of approximately 120 dB at a distance of 12 mm in air, using a 12 V voltage supply. The 2x2 array, assembled from four LN-based pMUT elements has a pitch size of 8 mm. By using the beamforming technique, the acoustic focal point of the array position within the plane at a 12 mm height can be controlled. Two phase angles, ψ and ϕ , are employed to adjust the x and y coordinates of the focal point, respectively, for the continuous movement of a particle within a 5 mm x 4 mm area. A lightweight foam particle with a mass of 0.7 mg and a radius of 1.8 mm is suspended 12 mm above the pMUT array by a thin wire. By adjusting the phase delay of ψ and ϕ , an acoustic radiation force of approximately 0.01 µN is applied on the foam particle for a movement of moving of about 1.8 mm. These findings validate the effectiveness of the proposed system by the beamforming technique for in-plane focal point control and the feasibility of using a pMUT array for mid-air particle manipulation. In the future, larger pMUT arrays, in combination with more complex beamforming techniques, are anticipated to achieve more precise particle manipulation in a broader spatial region and potentially counteract the force of gravity on particles.

ACKNOWLEDGEMENT

This work is supported in part by an NSF grant (ECCS-2128311) and the membership support of Berkeley Sensor and Actuator Center.

REFERENCES

- [1] S. van Wasen, Y. You, S. Beck, J. Riedel, D. A. Volmer, "Quantitative analysis of pharmaceutical drugs using a combination of acoustic levitation and high resolution mass spectrometry", *Analytical Chemistry*, 93,15 (2021).
- [2] L. E. Krushinski, L. Qiu, J. E. Dick, "Levitating Droplet Electroanalysis", *Analytical Chemistry* (2024).
- [3] S. Tsujino, T. Tomizaki, M. W. Kepa, "On-Demand Droplet Loading of Ultrasonic Acoustic Levitator with Small Droplets for Protein Crystallography Application", 2020 IEEE International Ultrasonics Symposium (2020), pp. 1-3,
- [4] M. A. Andrade, T. S. Ramos, J. C. Adamowski, A. Marzo, "Contactless pick-and-place of millimetric objects using inverted near-field acoustic levitation," *Applied Physics Letters*, 116, 5 (2020).
- [5] Q. Shi, W. Di, D. Dong, L. W. Yap, L. Li, D. Zang, W. Cheng, "A general approach to free-standing nanoassemblies via acoustic levitation self-assembly," ACS nano, 13, 5 (2019).
- [6] V. Contreras, K. Volke-Sepúlveda, "Enhanced standingwave acoustic levitation using high-order transverse modes in phased array ultrasonic cavities," *Ultrasonics*, 138, 107230 (2024).
- [7] J. F. P. Ospina, V. Contreras, J. Estrada-Morales, D. Baresch, J. L. Ealo, K. Volke-Sepúlveda, "Particle-size effect in airborne standing-wave acoustic levitation: Trapping particles at pressure antinodes," *Physical Review Applied*, 18, 3 (2022).
- [8] A. Marzo, S. A. Seah, B. W. Drinkwater, D. R. Sahoo, B. Long, S. Subramanian, "Holographic acoustic elements for manipulation of levitated objects," *Nature communications*, 6, 1 (2015).
- [9] S. Zehnter, M. A. Andrade, C. Ament, "Acoustic levitation of a Mie sphere using a 2D transducer array," *Journal of Applied Physics*, 129, 13 (2021).
- [10] F. Xia, Y. Peng, S. Pala, R. Arakawa, W. Yue, P. C. Tsao, C. M. Chen, H. Liu, M. Teng, J. H. Park, L. Lin, "High-SPL and Low-Driving-Voltage pMUTs by Sputtered Potassium Sodium Niobate," 2023 IEEE 36th International Conference on Micro Electro Mechanical Systems (2023), pp. 135-138.
- [11] W. Yue, Y. Peng, H. Liu, F. Xia, F. Sui, S. Umezawa, S. Ikeuchi, Y. Aida, L. Lin, "Auto-Positioning and Haptic Stimulations via A 35 mm Square Pmut Array," 2023 IEEE 36th International Conference on Micro Electro Mechanical Systems (2023), pp. 941-944.
- [12] F. Xia, H. Deng, W. Yue, Y. Peng, R. Arakawa, L. Lin, "PMUT Array for Mid-Air Thermal Display," 2023 IEEE International Ultrasonics Symposium (2023), pp. 1-3.
- [13] F. Pop, B. Herrera, M. Rinaldi, "Lithium Niobate Piezoelectric Micromachined Ultrasonic Transducers for high data-rate intrabody communication", *Nature* communications, 13, 1 (2022).
- [14] M. O'Donnell, E. T. Jaynes, J. G. Miller, "General relationships between ultrasonic attenuation and dispersion," *Journal of the Acoustical Society of America*, 63, 6 (1978).

CONTACT

*W. Yue; +1-510-984-8328; wei yue@berkeley.edu